Volume 1 | Number 1 | Jan 2013 | Pages 1–100

Nanoscale

www.rsc.org/nanoscale

ROYAL SOCIETY OF CHEMISTRY

www.rsc.org/nanoscale

Nanoscale

PAPER

Enhanced light out-coupling efficiency of organic light-emitting diodes with extremely low haze by plasma treated nanoscale corrugation

Ju Hyun Hwang,[a] Hyun Jun Lee,[a] Yong Sub Shim,[a] Cheol Hwee Park,[a] Sun-Gyu Jung,[a] Kyu Nyun Kim,[a] Young Wook Park,*[b] and Byeong-Kwon Ju*[a]

Extremely low-haze light extraction from organic light-emitting diodes (OLEDs) was achieved by utilizing nanoscale corrugation, which was simply fabricated with plasma treatment and sonication. The haze of the nanoscale corrugation for light extraction (NCLE) corresponds to 0.21% for visible
10 wavelengths, which is comparable to that of bare glass. The OLEDs with NCLE showed enhancements of 34.19% in current efficiency and 35.75% in power efficiency. Furthermore, the OLEDs with NCLE exhibited angle-stable electroluminescence (EL) spectra for different viewing angles, with no change to the Full Width at Half Maximum (FWHM) and peak wavelength. The flexibility of the polymer used for the NCLE and plasma treatment process indicates that the NCLE can be applied to large and flexible
15 OLED displays.

Introduction

Organic light-emitting diodes (OLEDs) have attracted a great deal of attention due to their high efficiency, fast response, flexible properties, color gamut, and potential as low-cost light
20 sources [1-3]. For practical OLEDs, phosphorescence is widely used owing to nearly 100% internal phosphorescence efficiency [4-5]. However, one of the major drawbacks of conventional OLEDs is about 80% loss of the light in the indium tin oxide (ITO)/organic mode, substrate mode, and surface plasmon mode
25 [6-7]. The mismatched refractive indices result in total internal reflection of the light, which limits the external quantum efficiency (EQE) to 20-30% [8]. Therefore, the efficient extraction of generated light is a critical requirement for achieving highly efficient OLEDs. There have been various
30 strategies for light extraction, such as Bragg diffraction gratings [9-12], low-index materials [13-14], scattering layers [15-16], substrate surface modifications [17-19], and microlens arrays (MLAs) [20-21].

Light extraction layers with periodic structures have been
35 widely explored to achieve highly efficient OLEDs. However, such periodic structures result in distorted emission spectra, and change the peak wavelength and Full Width at Half Maximum (FWHM) of the electroluminescence (EL) intensity. In addition, these periodic structures extract waveguided light only at specific
40 wavelengths or angles, which are dependent on the periodicity of the light-extraction layer [22-23]. Moreover, most fabrication processes are still complicated, expensive, and are limited to small-area OLEDs.

45 Another significant characteristic of a light extraction layer is a low haze. Although light extraction layers, such as microlens arrays and zinc oxide pillar arrays, have been used to extract waveguided light and achieve highly efficient OLEDs, the
50 resulting haze is so high that the OLEDs become blurred [24]. Thus, both highly enhanced efficiency and low haze are important properties in the field of OLED displays and OLED lighting.

In this study, we demonstrated a novel way of achieving the
55 OLEDs with a highly enhanced efficiency and extremely low haze by the nanoscale corrugation for light extraction (NCLE) between the ITO anode and glass substrate. The NCLE was easily fabricated with reactive ion etching (RIE) and a sonication process. The NCLE formed a corrugated surface that enhanced
60 the light scattering effect and diminished the microcavity effect. Since the NCLE with refractive index of 1.57-1.63 was fabricated between the ITO and EXG glass, the total internal reflection was reduced according to the Snell's law. The OLEDs with NCLE showed enhancements of 34.19% in current efficiency and 35.75%
65 in power efficiency. Furthermore, the OLEDs with NCLE exhibited angle-stable EL spectra for different viewing angles, with no change to the FWHM and peak wavelength, and like bare glass, extremely low haze for the entire visible spectrum. These characteristics of the NCLE can be applied to the field of OLED
70 displays and lighting. In addition, since the NCLE is fabricated through the plasma treatment of a flexible polymer, the NCLE can be adapted for large and flexible display applications.
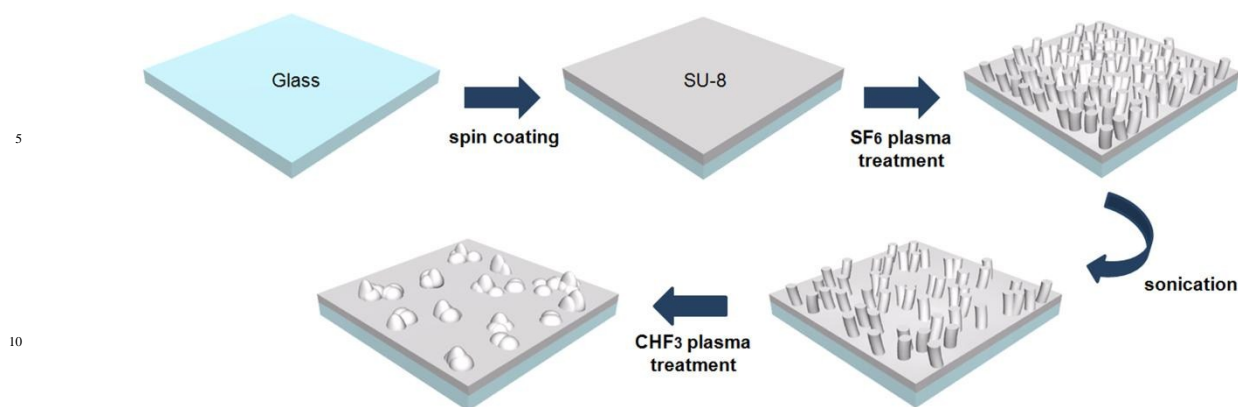
Figure 1. Schematic of the fabrication process of the nanoscale corrugation for light extraction (NCLE).

Experimental

Plasma nanotexturing has been used to fabricate columnar-like high aspect ratio structures. However, the structures produced by this technique are so sharp and dense that it could not be used to fabricate the light extraction layer in OLEDs [25]. The large surface roughness frequently resulted in the OLEDs having substantial leakage currents. Nanoscale structures with smooth surfaces and low density are essential for stable and highly efficient OLEDs, and they were easily fabricated with a combination of plasma etching and sonication.. The fabrication process of the nanoscale corrugation for the light extraction layer is shown in Figure 1. The polymer SU-8 (SU-8 2002, MicroChem) was spin-coated and then etched with RIE using a sulfur hexafluoride plasma. After the first etching of the polymer, the structures had a columnar-like high aspect ratio and high density. Sonication was applied to the structure to reduce the density of the structures. The surfaces of the nanoscale structures were smoothed with trifluoromethane plasma etching.

In order to investigate the properties of the NCLE, three different devices were fabricated. To obtain devices with different properties, the duration of the SF_6 plasma treatment was altered, while the other conditions (sonication duration and CHF_3 plasma treatment) remained unchanged.

The corrugated nanoscale layer between the glass and anode changed the topography of the organic layers and cathode. As a result, the waveguided light in the anode and organic layers was extracted through scattering induced by the changed topographies of the organic layers and cathode [26]. The ITO was deposited on the NCLE with radio frequency sputtering. The following layers were then thermally evaporated onto the ITO under vacuum conditions (2×10^{-6} Torr): a 60-nm-thick N,N'-bis(a-naphthyl)-N,N'-diphenyl-1,1'-biphenyl-4,4'-diamine layer for the hole transport layer, an 80-nm-thick tris-(8-hydroxyquinoline) aluminum layer for the light emission layer, a 0.8-nm-thick lithium fluoride layer for the electron injection layer, and a 100-nm-thick aluminum layer for the cathode.

X-ray photoelectron spectroscopy (XPS, PHI X-tool, ULVAC PHI Inc.) measurements were performed with monochromatized Al Kα X-rays (hν = 1486.6 eV). The surface morphologies and surface profiles were measured with scanning electron microscopy (SEM, S-4800, HITACHI Inc.) and atomic force microscopy (AFM, XE-100, Park system Inc.), respectively. The haze was evaluated with UV-VIS-NIR spectroscopy (Cary 5000, Agilent Technologies Inc.). The current-voltage characteristics were measured using a Keithley 237 High Voltage Source-Measure Unit (Keithley Instruments, Inc.), and the electroluminescence intensity was measured in a dark box using a spectroradiometer (PR-670 Spectra Scan, Photo Research, Inc.).
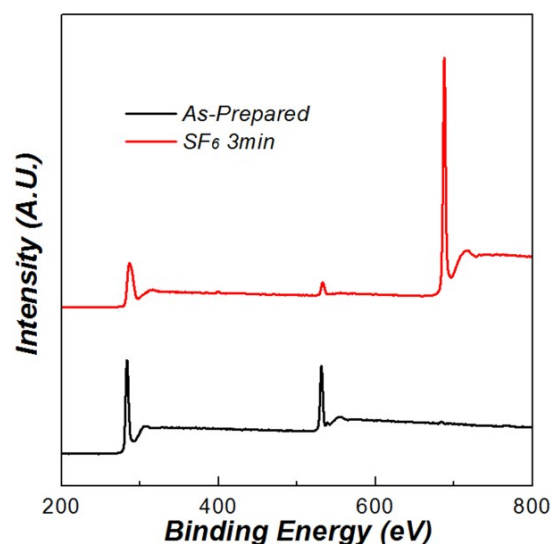
Results and discussion

Figure 2. XPS measurements of the as-prepared SU-8 and NCLE created by SF_6 plasma treatment for 3 min, sonication, and CHF_3 plasma.

Table 1 Atomic compositions of the as-prepared SU-8 and NCLE determined from XPS measurements.

	C (%)	O (%)	F (%)
As-prepared	74.9	21.8	0.5
SF_6 3min	50.7	3.9	45.0

XPS measurements were taken to determine the chemical composition of the polymer surface etched with the SF_6 plasma [27]. For the XPS measurements, the NCLE fabricated with the SF_6 plasma treatment for 3 min, sonication, and the CHF_3 treatment was used. The results of the XPS measurements are shown in Figure 2 and Table 1. The as-prepared SU-8 has a chemical composition of 74.9% C, 21.8% O, and 0.5% F, while the NCLE has a chemical composition of 50.7% C, 3.9% O, and 45.0% F. As can be seen, the plasma treatment and sonication process decreases the C and O content by 24.2% and 17.9%, respectively, and increases the F content by 44.5%. This change in the chemical composition means that the SF_6 plasma and CHF_3 plasma partially removes C and O from the as-prepared SU-8, and replaces them with F. The increased F content is a result of the SF_6 and CHF_3 plasmas treatment as a source of F.

It is desirable to select a nanoscale structure size and periodicity that is comparable to the wavelength of light to maximize the out-coupling of the light [23]. SEM was used to measure the surface topography of the NCLE. Figure 3 shows the SEM images of the various NCLE fabricated. The three NCLE shown had SF_6 plasma treatment durations of 2, 3, and 4 min (denoted NCLE 2, NCLE 3, and NCLE 4, respectively), while the conditions of the other processes remained unchanged. The images show that as the plasma treatment duration increases, the height of the NCLE structures increases. The RMS-roughness becomes saturated for higher plasma dose owing to the competition between the etching and reformation [28].

AFM was used to quantify the topography of the different NCLE. Figure 4 shows surface profiles, and 2- and 3-dimensional AFM surface images from left to right. As the duration of the SF_6 plasma treatment increases from 2 to 4 min, the height, width, and periodicity of the nano-structures also increase.
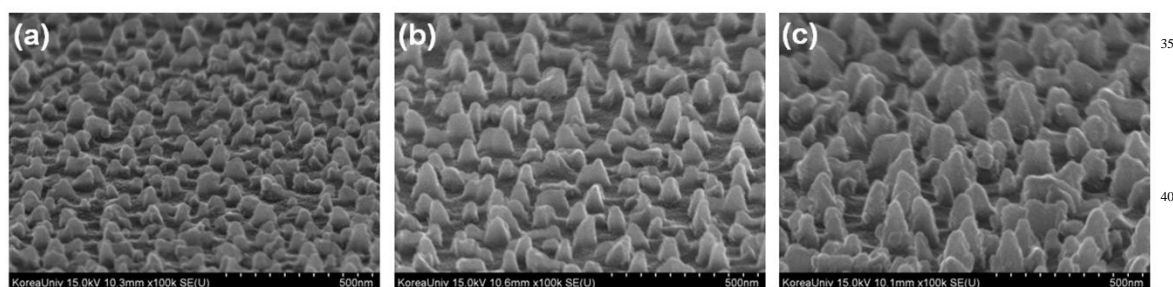

Figure 3. SEM images of various NCLE on glass substrates formed by SF_6 plasma treatment, sonication, and CHF_3 plasma treatment. The duration of the SF_6 plasma treatment was altered to create the different NCLE: (a) 2 min, (b) 3 min, and (c) 4 min. The conditions of the other processes remained unchanged.
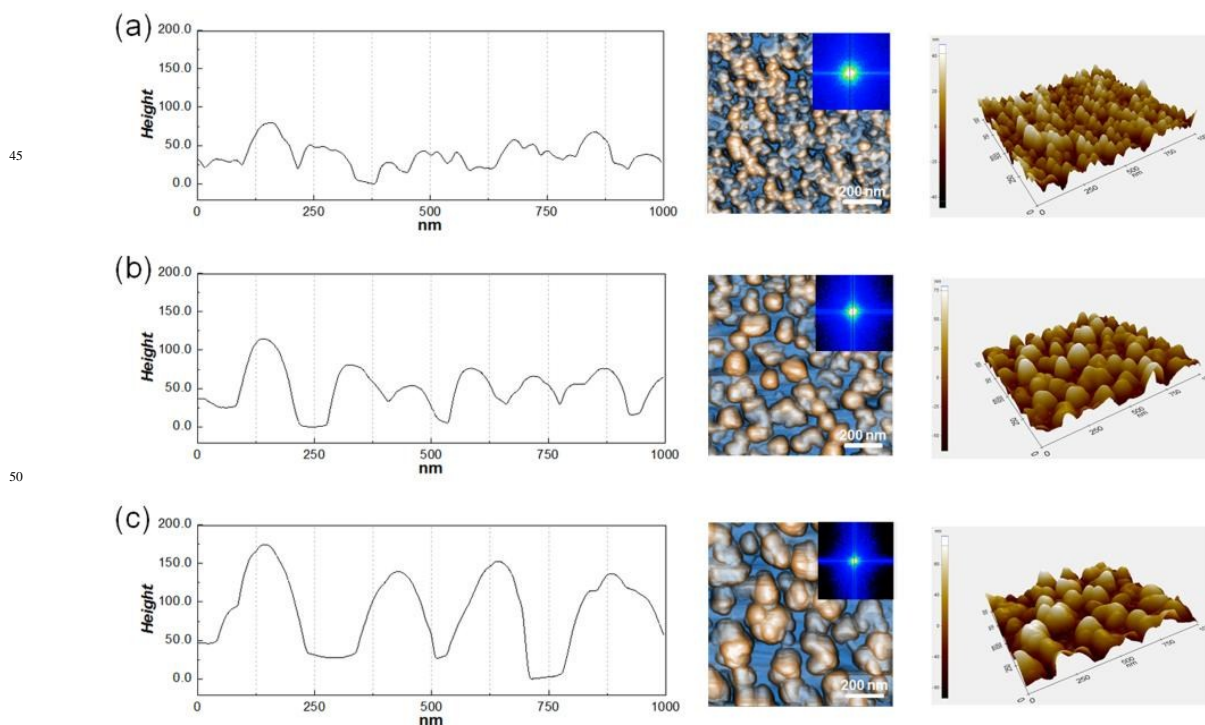

Figure 4. Surface profiles, and two- and three-dimensional AFM surface images of (a) NCLE 2, (b) NCLE 3, and (c) NCLE 4. The insets are fast Fourier transforms of each NCLE.
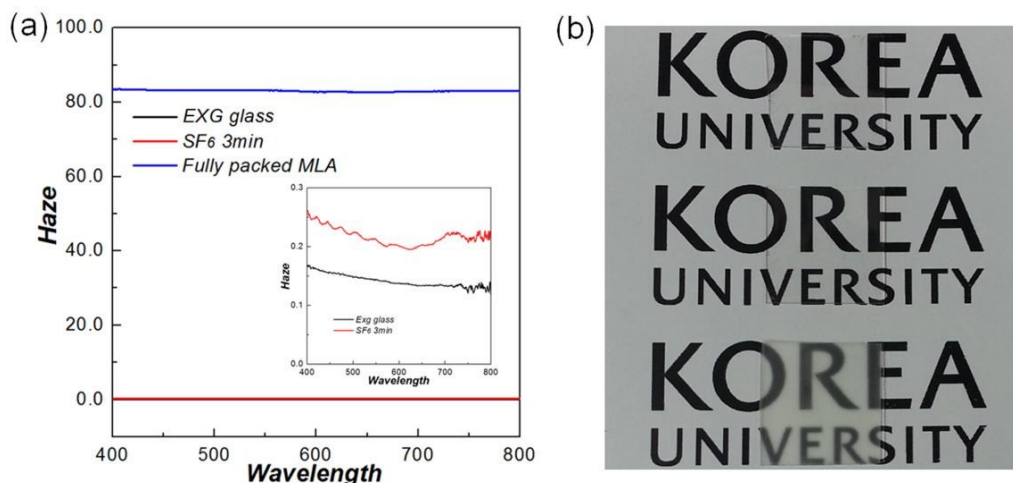
Figure 5. a) Comparison of the resulting haze of EXG glass, NCLE 3, and fully packed MLAs as a function of wavelength. b) Photograph of the EXG glass (top), NCLE 3 (middle), and fully packed MLAs (bottom).

The height of the NCLE 2, NCLE 3, and NCLE 4 range from 10-80 nm, 10-110 nm, and 20-180 nm, respectively. The width of the structures range from 20-120 nm (NCLE 2), 110-130 nm (NCLE 3), and 140-230 nm (NCLE 4). The inset images in the 2D AFM images are the fast Fourier transforms (FFTs) of each NCLE. The FFTs resulted in vaguely symmetrical rings, which means that the NCLE have a range of diameters with randomly dispersed orientations.

Figure 5 shows the haze of Eagle XG (EXG) glass, NCLE 3, and fully packed MLAs as a function of wavelength, as well as a photograph of these substrates. The inset in Figure 5a shows the haze magnification of EXG glass and NCLE 3. The haze was calculated with the following equation

$$Haze = \frac{\text{Total transmittance} - \text{specular transmittance}}{\text{Total transmittance}}$$

Scattering media usually increase the haze of the light because the light scatters in all directions. In display applications, this increased haze blurs the pixels and ruins the resolution of the device [29]. The haze at 525 nm resulting from the EXG glass, NCLE 3, and fully packed MLAs is 0.14%, 0.21%, and 83.58%, respectively. The haze of the NCLE 3 is only 0.07% higher than that of the EXG glass, which means that there is no significant difference in clarity between the EXG glass and NCLE 3.

The current density of OLEDs as a function of the applied voltage is shown in Figure 6a. As can be seen, the current density increases as the height and width of the NCLE increases. This is because the nanoscale corrugation increases the effective surface area and decreases the thickness of the organic layers [30-32]. Although the current density increases, the higher enhancement of the luminance in the OLEDs with NCLE indicates extraction of the waveguide light (see Supporting Information). The nanoscale corrugation enhances the intensity of the electric field in the corrugated anode, which increases the current density of a device with NCLE. Figure 6b shows the current and power efficiencies as a function of current density. The device with higher and wider NCLE exhibits improved current and power efficiencies. The current efficiencies of the devices are 3.19 cd/A (Ref), 3.62 cd/A (NCLE 2), and 4.28 cd/A (NCLE 3) at 1000 cd/m^2, while their power efficiencies are 1.79 lm/W (Ref), 2.03 lm/W (NCLE 2), and 2.43 lm/W (NCLE 3) at 1000 cd/m^2. The improved performances of the devices with NCLE correspond to enhancements of 13.48% (NCLE 2) and 34.19% (NCLE 3) in current efficiency and 13.41% (NCLE 2) and 35.75% (NCLE 3) in power efficiency.
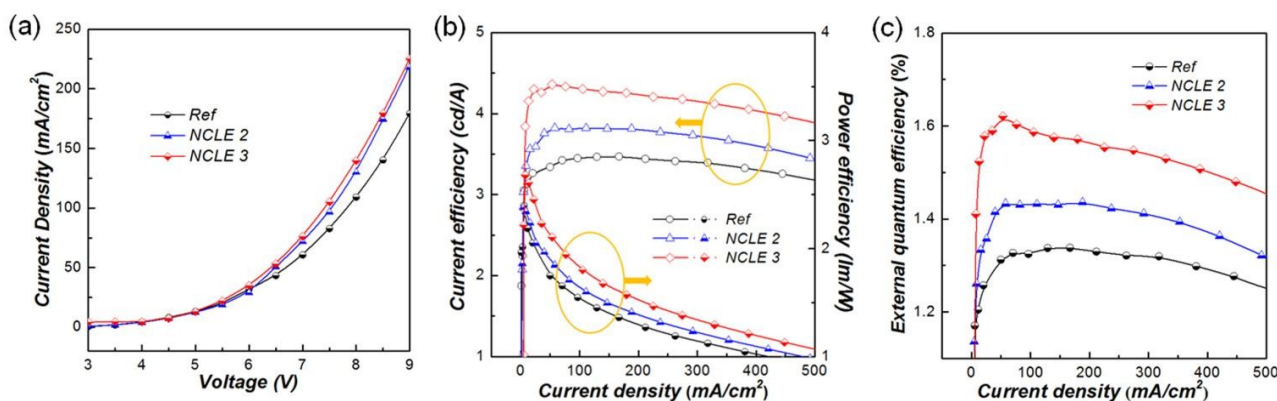

Figure 6. Device performance of typical OLEDs without NCLE for reference (black), and OLEDs with NCLE 2 (blue) and NCLE 3 (red): a) current density as a function of voltage, b) current and power efficiencies as a function of current density, and (c) external quantum efficiency as a function of current density.
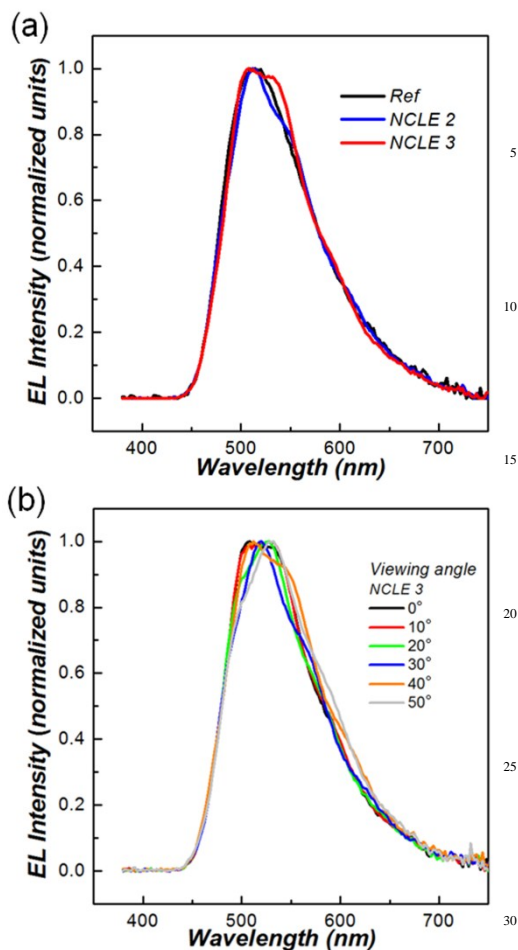
Figure 7. a) Normalized electroluminescence intensity as a function of the wavelength without NCLE for reference (black), and with NCLE 2 (blue) and NCLE 3 (red). b) Normalized spectral emission intensity for the OLEDs with NCLE 3 at different viewing angles.

Figure 6c shows the external quantum efficiency plotted as a function of the current density. The external quantum efficiency at 50 mA/cm^2 is 1.3% for the reference device, 1.42% for NCLE 2, and 1.61% for NCLE 3. The improved efficiencies correspond to enhancements of 9.23% (NCLE 2) and 19.25% (NCLE 3). The higher and wider NCLE 3 extracts much more waveguided light than the NCLE 2 and reference devices. This is in agreement with the improved current and power efficiencies for the higher and wider NCLE. The enhancement is caused by the strong scattering effect of the higher NCLE. The scattering effect of the NCLE increases with the height of the NCLE, but if the height is too great, the NCLE can also cause device failure through the creation of paths that allow current leakage. For example, the NCLE 4 with a peak-valley roughness, R_{pv}, of 180 nm results in the device short-circuiting. Another reason for the improved light extraction effect of the NCLE is the relatively well-matched refractive indices of the NCLE and glass substrate. The refractive indices of ITO, NCLE and EXG glass for 380-700 nm are approximately 1.82-2.08, 1.57-1.63 and 1.50-1.52, respectively. Without the NCLE, the light generated in the emission layer passes directly from the ITO to the EXG glass, which results in large total internal reflection loss due to a big difference of refractive index. But when the NCLE with refractive index of 1.57-1.63 is fabricated between the ITO and EXG glass, the total internal reflection loss was reduced according to the Snell's law.

An internal light extraction layer with a 2-dimensional photonic crystal structure changes the emission spectrum and the shape of the peak emission because of Bragg scattering modes and the microcavity mode [33]. Figure 7a shows the normalized electroluminescence intensities of the three devices as a function of wavelength. The wavelength of the peak EL intensity for all three devices is 513 nm and the FWHM is also same as 101 nm in all three devices. Although there is a slight distortion of the normalized EL intensity between 524 and 552 nm for NCLE 3, the overall tendency of the normalized EL intensity across the entire visible spectrum is similar for all devices. The similarity of the normalized EL intensities means that the microcavity effect in the OLEDs is reduced by the NCLE because of its irregular topography.

The normalized EL intensities as a function of wavelength at different viewing angles are shown in Figure 7b. The emission intensity of conventional OLEDs with ITO anodes is dependent on the viewing angle [34]. However, the emission intensity dependence of NCLE 3 on the viewing angle is very small. The NCLE suppresses the color shift of the device through the re-distribution of photons by scattering [35-36]. The peak wavelength of NCLE 3 slightly increases to longer wavelengths as the viewing angle increases, with the shift range less than 24 nm. At the right side of the plots, the EL intensity oscillates with no specific trend. This is a result of the combined effects of the existing microcavity and scattering.

Conclusions

OLEDs with highly efficient internal light extraction and angle-stable EL spectra have been developed by using a simple and easy manufacturing process. The nanoscale structures for light extraction form a corrugated surface that enhances the light scattering effect and diminishes the microcavity effect. The NCLE with refractive index of 1.57-1.63 is fabricated between the ITO and EXG glass, and thus, the total internal reflection loss is reduced according to the Snell's law. These properties enhance the current efficiency by 34.19% and the power efficiency by 35.75%. Furthermore, the OLEDs with NCLE exhibited angle-stable EL spectra for the entire visible spectrum at different viewing angles, with no change to the FWHM and peak wavelength. In addition, the NCLE on a glass substrate showed extremely low haze in the visible spectrum, which is comparable to that of bare glass. The NCLE were fabricated with reactive ion etching, which allows NCLE to be applied to large-area OLEDs. Moreover, since the polymer used to create the NCLE is flexible, the NCLE can be adapted for use in flexible display applications.

Acknowledgements

Notes and References

[a] *Display and Nanosystem Laboratory, College of Engineering, Korea University, Seoul 136-713, Republic of Korea,*
E-mail: bkju@korea.ac.kr; Fax: +82-3290-3671; Tel: +82-3290-3237
[b] *The Institute of High Technology Materials and Devices, Korea University, Seoul 136-713, Republic of Korea,*
E-mail: zerook@korea.ac.kr; Fax: +82-3290-3671; Tel: +82-3290-3665

1. S. Reineke, F. Lindner, G. Schwartz, N. Seidler, K. Walzer, B. Lüssem, and K. Leo, *Nature*, 2009, **459**, 234-238.
2. Y. Sun and S. R. Forrest, *Nat. Photonics*., 2008, **2**, 483-487.
3. B. W. D'Andrade and S. R. Forrest, *Adv. Mater*., 2004, **16**, 1585-1595.
4. C. Adachi, M. A. Baldo, M. E. Thompson, and S. R. Forrest, *J. Appl. Phys*., 2001, **90**, 5048.
5. Y. Sun, N. C. Giebink, H. Kanno, B. Ma, M. E. Thompson, and S. R. Forrest, *Nature*, 2006, **440**, 908-912.
6. C. Lee, D. J. Kang, H. Kang, T. Kim, J. Park, J. Lee, S. Yoo, and B. J. Kim, *Adv. Energy Mater*., 2014, **4**, 1301345.
7. B. C. Krummacher, S. Nowy, J. Frischeisen, M. Klein, and W. Brütting, *Org. Electron*., 2009, **10**, 478-485.
8. A. Chutinan, K. Ishihara, T. Asano, M. Fujita, and S. Noda, *Org. Electron*., 2005, **6**, 3-9.
9. D. K. Gifford and D. G. Hall, *Appl. Phys. Lett*., 2002, **81**, 4315.
10. B. J. Matterson, J. M. Lupton, A. F. Safonov, M. G. Salt, W. L. Barnes, and I. D. W. Samuel, *Adv. Mater*., 2001, **13**, 123-127.
11. S. M. Jeong, F. Araoka, Y. Machida, K. Ishikawa, H. Takezoe, S. Nishimura, and G. Suzaki, *Appl. Phys. Lett*., 2008, **92**, 083307.
12. K. Ishihara, M. Fujita, I. Matsubara, T. Asano, S. Noda, H. Ohata, A. Hirasawa, H. Nakada, and N. Shimoji, *Appl. Phys. Lett*., 2007, **90**, 111114.
13. T. W. Koh, J. M. Choi, S. Lee, and S. Yoo, *Adv. Mater*., 2010, **22**, 1849-1853.
14. T. Tsutsui, M. Yahiro, H. Yokogawa, K. Kawano, and M. Yokoyama, *Adv. Mater*., 2001, **13**, 1149-1152.
15. B. Riedel, Y. Shen, J. Hauss, M. Aichholz, X. Tang, U. Lemmer, and M. Gerken, *Adv. Mater*., 2011, **23**, 740-745.
16. Y. Gu, D. D. Zhang, Q. D. Ou, Y. H. Deng, J. J. Zhu, L. Cheng, Z. Liu, S. T. Lee, Y. Q. Li, and J. X. Tang, *J. Mater. Chem. C*., 2013, **1**, 4319-4326.
17. Y. H. Cheng, J. L. Wu, C. H. Cheng, K. C. Syao, and M. C. M. Lee, *Appl. Phys. Lett*., 2007, **90**, 091102.
18. Y. Sun and S. R. Forrest, *J. Appl. Phys*., 2006, **100**, 073160.
19. H. J. Peng, Y. L. Ho, X. J. Yu, and H. S. Kwok, *J. Appl. Phy*., 2004, **96**, 1649.
20. J. B. Kim, J. H. Lee, C. K. Moon, S. Y. Kim, and J. J. Kim, *Adv. Mater*., 2013, **25**, 3571-3577.
21. T. W. Koh, H. Cho, C. Yun, and S. Yoo, *Org. Electron*., 2012, **13**, 3145-3153.
22. J. M. Ziebarth, A. K. Saafir, S. Fan, and M. D. McGehee, *Adv. Func. Mater*., 2004, **14**, 451-456.
23. Y. R. Do, Y. C. Kim, Y. W. Song, C. O. Cho, H. Jeon, Y. J. Lee, S. H. Kim, and Y. H. Lee, *Adv. Mater*., 2003, **15**, 1214-1218.
24. S. Möller and S. R. Forrest, *J. Appl. Phys*., 2002, **91**, 3324.
25. K. Tsougeni, N. Vourdas, A. Tserepi, and E. Gogolides, *Langmuir*, 2009, **25**, 11745-11759.
26. W. H. Koo, S. M. Jeong, F. Araoka, K. Ishikawa, S. Nishimura, T. Toyooka, and H. Takezoe, *Nat. Photonics*, 2010, **4**, 222-226.
27. S. G. Park, J. H. Moon, H. C. Jeon, and S. M. Yang, *Soft Matter*, 2012, **8**, 4567-4570.
28. F. Walther, P. Davydovskaya, S. Zurcher, M. Kaiser, H. Herberg, A. Gigler, and R. W. Stark, *J. Micromech. Microeng*., 2007, **17**, 524-531.
29. C. Lee and J. J. Kim, *Small*, 2013, **9**, 3858-3863.
30. X. L. Zhang, J. Feng, J. F. Song, X. B. Li, and G. B. Sun, *Opt. Lett*., 2011, **36**, 3915-3917.
31. A. O. Altun, S. Jeon, J. Shim, J. H. Jeong, D. G. Choi, K. D. Kim, J. H. Choi, S. W. Lee, E. S. Lee, H. D. Park, J. R. Youn, J. J. Kim, Y. H. Lee, J. W. Kang, *Org. Electron*., 2010, **11**, 711-716.
32. Y. Luo, L. Wang, Y. Ding, L. Li, and J. Shi., *Opt. Lett*., 2013, **38**, 2394-2396.
33. Y. R. Do, Y. C. Kim, Y. W. Song, and Y. H. Lee, *J. Appl. Phys*., 2004, **96**, 7629.
34. Y. H. Kim, J. Lee, W. M. Kim, C. Fuchs, S. Hofmann, H. W. Chang, M. C. Gather, L. Müller-Meskamp, and K. Leo, *Adv. Funct. Mater*., 2014, **24**, 2553-2559.
35. K. Hong, H. K. Yu, I. Lee, K. Kim, S. Kim, and J. L. Lee, Adv. *Mater*., 2010, **22**, 4890-4894.
36. T. Nakamura, H. Fujii, N. Juni, and N. Tsutsumi, *Opt. Rev*., 2006, **13**, 104-110.